Journal of Molecular Structure 1010 (2012) 116–122

Contents lists available at SciVerse ScienceDirect

Journal of Molecular Structure

journal homepage: www.elsevier.com/locate/molstruc

Synthesis and fluorescence properties of Tb(III) complex with a novel β-diketone ligand as well as spectroscopic studies on the interaction between Tb(III) complex and bovine serum albumin

Zhenfeng Zhang, Ruiren Tang *

School of Chemistry and Chemical Engineering, Central South University, Hunan 410083, PR China

ARTICLE INFO

Article history:
Received 24 October 2011
Received in revised form 24 November 2011
Accepted 24 November 2011
Available online 1 December 2011

Keywords:
Aromatic β-diketone
Lanthanide complex
Fluorescence property
Bovine serum albumin (BSA)

ABSTRACT

A novel aromatic β-diketone ligand, 4-isopropyl-2,6-bisbenzoylactyl pyridine (L), and its corresponding Tb(III) complex $Tb_2(L)_3{\cdot}5H_2O$ were synthesised in this paper. The ligand was characterized by FT-IR and ^1H NMR. The complex was characterized with elemental analysis and FT-IR. The investigation of fluorescence property of the complex showed that the Tb(III) ion could be sensitized efficiently by the ligand. Furthermore, the interaction of $Tb_2(L)_3{\cdot}5H_2O$ with bovine serum albumin (BSA) has been investigated by fluorescence quenching spectra, UV–vis absorbance and synchronous fluorescence spectra. The fluorescence quenching mechanism of BSA by $Tb_2(L)_3{\cdot}5H_2O$ was analyzed. The binding constants, binding site number and the corresponding thermodynamic parameters at different temperatures were calculated. The results indicated that the Van der Waals and hydrogen bond interactions were the predominant intermolecular forces in stabilizing the complex. Moreover, the effect of $Tb_2(L)_3{\cdot}5H_2O$ on the conformation of BSA was analyzed according to synchronous fluorescence.

1. Introduction

Within recent years, luminescent lanthanide–organic frameworks have attracted significant attention due to their absorbing architectures and enormous potential applications in many areas, such as light emitting diode [1], luminescence probes or sensors [2,3]. The absorption and emission spectra intensity of the trivalent rare earth ions (RE(III)) is weak since intra-configuration 4f–4f transitions in trivalent lanthanide ions are forbidden (Laporte rule). In order to overcome this drawback and obtain outstanding luminescent properties, an organic ligand with excellent absorption coefficient and high efficient ligand-to-RE(III) ions energy transfers, which acts as an "antenna" [4] is very necessary. Based on the different ligands and the central RE(III), many novel ligands and complexes have been designed and synthesised [5]. The main ligands include aromatic carboxylic acid, 1,10-phenanthroline (phen), pydine and β-diketone, etc. [6–8]. Among these ligands, aromatic β-diketone compounds have been more attractive for their highly efficient intermolecular energy transfers [9,10].

It is well known that serum albumin is the most abundant protein in plasma, playing the most important physiological role in the maintenance of colloid osmotic blood pressure and in the binding and transportation of various ligands such as fatty acids, hormones, and drugs [11]. Recently, the interactions of serum albumin with lanthanide complexes have received much interest owing to their application in a great deal of medical and chiroptical systems [12,13]. The luminescent Eu and Tb complexes are capable of selectively binding to 'drug site II' of serum albumin and playing a significant part in drug pharmacokinetics and pharmacodynamics [12]. In addition, bovine serum albumin (BSA) has been studied as a model protein due to its structural homology with human serum albumin (HSA) [14].

Accordingly, in this work, a novel aromatic β-diketone ligand of 4-isopropyl-2, 6-bisbenzoylactyl pyridine (L) with large conjugated plane and rigid structure, was designed and synthesised (Scheme 1). And its corresponding Tb(III) complex was also prepared. The fluorescence property of the complex was investigated in detail. Furthermore, the information related to the binding mechanisms with BSA, such as binding modes, binding constants, and quenching rate constants, was explored by UV–vis and fluorescence measurements.

2. Experimental

2.1. Materials

Isobutylaldehyde was purchased from Jiangsu (China) Medicine Co. Ltd., BSA, obtained from Sigma Chemical Co. Ltd., was dissolved in 0.1 M Tris–HCl buffer solution (pH = 7.40, 50 mM NaCl). BSA stock solution (1.0×10^{-5} M) was kept in the fridge at 0–4 °C.

* Corresponding author. Tel.: +86 731 8883691; fax: +86 731 88879616.
E-mail address: trr@mail.csu.edu.cn (R. Tang).

0022-2860/$ - see front matter © 2011 Elsevier B.V. All rights reserved.
doi:10.1016/j.molstruc.2011.11.041

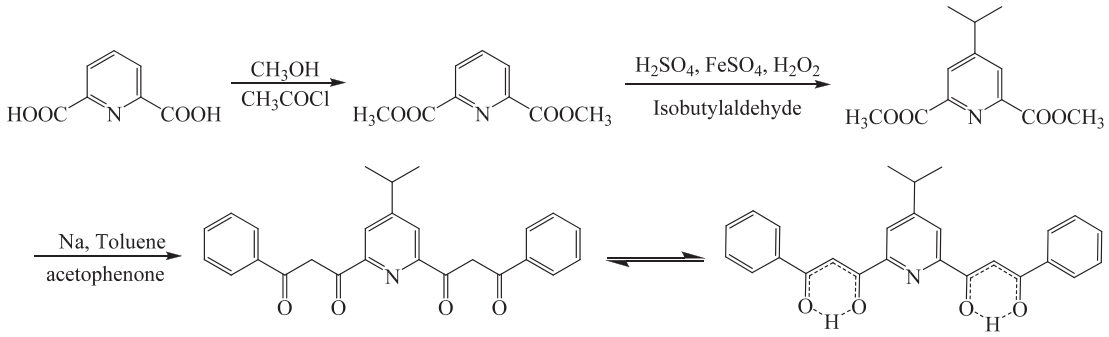

Scheme 1. Synthetic route of ligand L.

The complex $Tb_2(L)_3{\cdot}5H_2O$ was dissolved in ethanol to form 1 mM stock solution. And other chemicals were of A.R. grade without further purification. Doubly distilled and deionized water was used in the whole experiments.

2.2. Methods

Melting points were determined on a XR-4 apparatus (thermometer uncorrected); elemental analysis was carried out by a Perkin Elmer 2400 elemental analyzer; infrared spectra were recorded on a Nicolet NEXUS 670 FT-IR spectrophotometer using KBr discs in the 400–4000 cm^{-1} region; ^1H NMR spectra were measured with a Bruker-400 MHz nuclear magnetic resonance spectrometer with $CDCl_3$ as solvent and TMS as internal reference. The UV–vis spectra were recorded on an UV-2450 spectrophotometer. Luminescence measurements were made on a Hitich F-4600 spectrophotometer, the widths of both the excitation and emission slit were set to 5 nm with the photomultiplier tube voltage at 700 V.

2.3. Synthesis of the ligand

2.3.1. Synthesis of dimethyl 4-isopropyl-2,6-pyridinedicarboxylate

The synthesis of ligand referred to the previously reported method [15]. Briefly, to a mixture of dimethyl 2,6-pyridinedicarboxylate (4.9 g, 25 mmol), isobutylaldehyde (5.4 g, 75 mmol) and H_2SO_4 (w/w, 30% aqueous solution, 36 mL), aqueous solution of $FeSO_4$ (4.9 g, 30 mmol) and H_2O_2 (w/w, 30% aqueous solution, 40 mL) were added dropwise under vigorous stirring over 15 min at 0 °C. The reaction mixture was stirred for an additional 15 min, treated with K_2CO_3 powder to pH 2, and extracted with chloroform (3 × 35 mL). The combined extracts were dried, evaporated, and purified by flash chromatography to give white needles of dimethyl 4-isopropyl-2,6-pyridinedicarboxylate (3.9 g, yield: 66%) m.p. 58–60 °C; IR: υ_{max} = 3081, 2954, 2878, 1719, 1600, 1558, 1443, 1358, 1331, 1216 cm^{-1}; ^1H NMR (400 MHz, $CDCl_3$): δ = 1.35 (d, J = 8 Hz, 6 H), 3.07 (m, J = 8 Hz, 1 H), 4.02 (s, 6 H), 8.17 ppm (s, 2 H).

2.3.2. Synthesis of the ligand (4-isopropyl-2,6-bisbenzoylactyl pyridine)

Sodium metal (0.92 g, 40 mmol) was added to a solution of dimethyl 4-isopropyl-2,6-pyridinedicarboxylate (2.37 g, 10 mmol) in 20 mL dry toluene, and then a solution of acetophenone (4.8 g, 40 mmol) in 10 mL dry toluene was added dropwise under stirring at 60 °C for 4 h. The sodium salt was collected by filtration, washed with petroleum ether. The dried solid was added to dilute hydrochloric acid (2.0 M) and the resulting precipitate was collected by filtration. The crude products were recrystallized over methanol to give the title compound (L) (3.06 g, yield: 74%). m.p. 178–180 °C; IR: υ_{max} = 3459, 3054, 2965, 1611, 1571, 1487, 1342, 687 cm^{-1}; ^1H NMR (400 MHz, $CDCl_3$): δ = 1.35 (d, J = 8 Hz, 6 H), 3.05(m, J = 8 Hz, 1 H), 7.53–8.10 (m, J = 8 Hz, 10 H), 8.1 (s, 2 H). 16.35 ppm (s, 2 H).

2.4. Synthesis of the Tb(III) complex

A solution of $TbCl_3$ (0.4 mmol) in ethanol (5 mL) was added to the mixture of ligand L (0.6 mmol) in ethanol (5 mL). And the resulting mixture was treated with aqueous NaOH (0.1 M) to pH 6, and stirred at 60 °C for 24 h. The resulting yellow precipitate was collected by filtration, washed with the mixture solution of ethanol and chloroform mixture (v:v, 1:1), and dried in vacuum to give a yellow solid.

2.5. Interaction of complex with BSA

2.5.1. Fluorescence spectroscopy

To 2 mL of BSA stock solution in a 1 cm quartz cell, the complex $Tb_2(L)_3{\cdot}5H_2O$ working solution was gradually added using a pipette. The accumulated volumes were 0, 10, 15, 20, 30, 35, 40, 50, 75 and 100 μL. The quenching of the emission intensity of BSA at around 340 nm was observed with the increased concentration of the complex. Fluorescence spectra were recorded from 300 to 460 nm at an excitation wavelength of 280 nm at three temperatures (291 K, 298 K, and 310 K). Both of the excitation and emission slit widths were 5 nm.

2.5.2. UV–vis absorption spectroscopy

Absorption spectra (UV) measurements were made by using a Shimadzu 2450 UV–Vis spectrophotometer at 298 K in the region of 260–300 nm. The 2.0 mL of BSA stock solution was titrated with successive additions of the complex $Tb_2(L)_3{\cdot}5H_2O$ working solution. The Tris–HCl buffer solution was used as a reference solution.

3. Results and discussion

3.1. Composition and properties of the complex

The elemental analytical data for the complex was presented in Table 1, which was in good agreement with the values calculated, indicating that the composition of the complex was confirmed to be $Tb_2(L)_3{\cdot}5H_2O$. The complex was yellowish powder, stable under atmospheric condition and soluble in H_2O, ethanol, DMF, DMSO and acetone.

3.2. FT-IR spectra

The FT-IR spectra and characteristic absorption bands of the free ligand L and its Tb(III) complex were shown in Fig. 1 and Table 2, respectively. In the free ligand L, the weak band at 3459 cm^{-1}

Table 1
Composition analytical data for the complex/%.

Complex	C found (calc.)	H found (calc.)	N found (calc.)	Tb found (calc.)
$Tb_2(L)_3{\cdot}5H_2O$	56.18 (56.22)	4.83 (4.75)	2.58 (2.52)	20.07 (20.18)

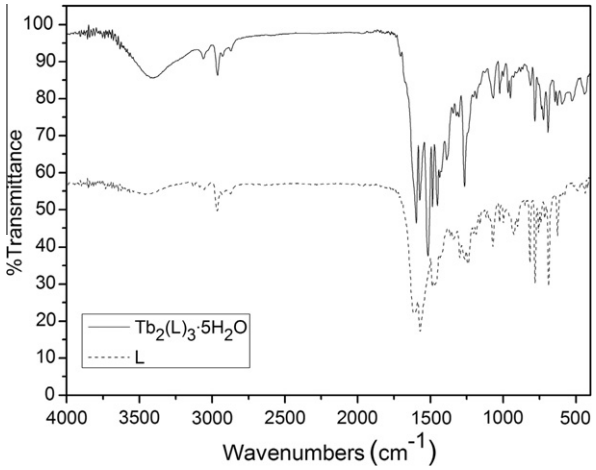

Fig. 1. IR spectra of ligand L and complex $Tb_2(L)_3{\cdot}5H_2O$.

Table 2
Characteristic IR bands (cm^{-1}) of the ligand L and the complex $Tb_2(L)_3{\cdot}5H_2O$.

Sample	υ(O–H)	υ(C=O)	υ(C=C)	υ(C=N)	υ(C–O)
L	3459	1611	1533	1571	1298 1263
$Tb_2(L)_3{\cdot}5H_2O$	3422	1597	1517	1573	1266

can be attributed to the υ(O–H) and the enol-isomer υ(C=O) vibration is at 1611 cm^{-1}. However, the keto-isomer υ(C=O) vibration at 1640 cm^{-1} was not be observed, indicating that six-membered ring was constructed by the intramolecular hydrogen bond generated from the two carbonyl groups of the ligand [16]. In the complex of $Tb_2(L)_3{\cdot}5H_2O$, the υ(C=O) peak of enol-isomer is shifted downfield to 1597 cm^{-1}, which suggests that the carbonyl group may participate in coordination reaction. In addition, high intensity sharp bands are observed at 1517 cm^{-1} and 1266 cm^{-1} which are attributed to υ(C=C) and υ(C–O), respectively, indicating that the enol-form anion of ligand is coordinated to Tb(III) ion [17]. The υ(C=N) peak is slightly shifted (1571 cm^{-1} for the ligand L, 1573 cm^{-1} for the complex $Tb_2(L)_3{\cdot}5H_2O$), which suggests that pyridine nitrogen atom doesn't participate in coordination reaction. The absorption band assigned to the coordinated Tb–O was found at around 436 cm^{-1}. The band υ(O–H) vibration at 3422 cm^{-1} is relatively intense and can be assigned to solvated water. However, the $\rho_\gamma(H_2O)$ and $\rho_\omega(H_2O)$ bands at approximately 850 cm^{-1} and 650 cm^{-1} were not observed in the spectra of the complex, indicating that there was no coordinated water molecules [18].

The results of elemental analysis and IR spectroscopy indicated that the enol-forms of the ligand L was only involved with the coordination, and we suspected that the chemical structure of complex may be as shown in Scheme 2.

3.3. Luminescence properties

The fluorescence characteristics data of the solid complex $Tb_2(L)_3{\cdot}5H_2O$ at room temperature are listed in Table 3. The corresponding excitation and emission spectra are shown in Fig. 2.

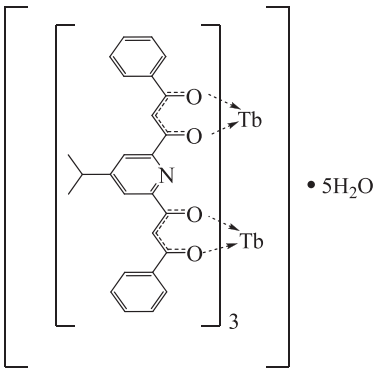

Scheme 2. Chemical structure of $Tb_2(L)_3{\cdot}5H_2O$.

Table 3
Fluorescence spectra date for the complex $Tb_2(L)_3{\cdot}5H_2O$.

complex	λ_{ex} (nm)	λ_{em} (nm)	FI[a]	Assignment
$Tb_2(L)_3{\cdot}5H_2O$	274	491	2241	$^5D_4 \rightarrow {}^7F_6$
		546	3773	$^5D_4 \rightarrow {}^7F_5$
		587	1045	$^5D_4 \rightarrow {}^7F_4$
		623	485	$^5D_4 \rightarrow {}^7F_3$

[a] Fluorescence intensity.

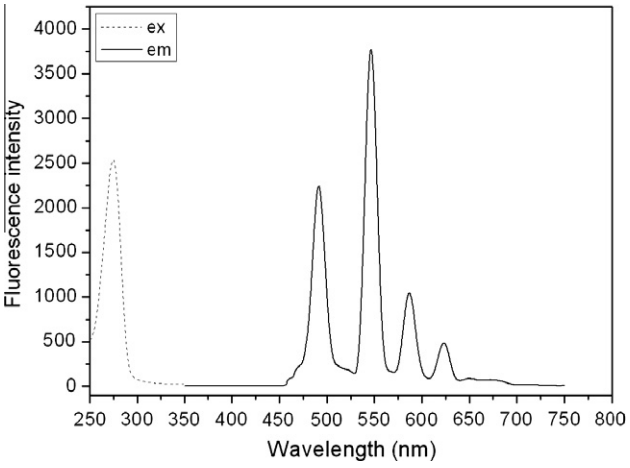

Fig. 2. The excitation and emission spectra of $Tb_2(L)_3{\cdot}5H_2O$.

The maximum excitation wavelength of the complex $Tb_2(L)_3{\cdot}5H_2O$ is 274 nm, due to the π–π* transition centered at the ligand L. The complex displays the characteristic line emission of 4f–4f transition of Tb(III) ion, consisting of four main lines at 491 nm ($^5D_4 \rightarrow {}^7F_6$), 546 nm ($^5D_4 \rightarrow {}^7F_5$), 587 nm ($^5D_4 \rightarrow {}^7F_4$), and 623 nm ($^5D_4 \rightarrow {}^7F_3$) (Fig. 2). There is no trace emission from ligand L (about 450 nm) in the complex, which shows that an efficient energy transfer in the complex system occurs from the singlet excited state of the ligand L to the singlet excited state of β-diketone unit, and followed by intersystem crossing to the excited triplet state of β-diketone unit, where it is finally transferred to the central Tb(III) ion. Therefore, Tb(III) ion emits characteristic luminescence. Due

to the presence of a scattering signal at 491 nm, and the $^5D_4 \rightarrow {}^7F_5$ emission is a magnetic dipole transition, which is less affected by the ligand field, so the peak height at 546 nm for terbium was used to measure the fluorescence intensities. The fluorescence emission maximum at 546 nm is observed. The emission band ($^5D_4 \rightarrow {}^7F_5$) is obviously stronger than the other emission bands ($^5D_4 \rightarrow {}^7F_6$, $^5D_4 \rightarrow {}^7F_4$, $^5D_4 \rightarrow {}^7F_3$) (Fig. 2). The typical narrow emission bands of Tb(III) ion can be detected upon excitation of the ligand-centered absorption band, indicating that the ligand is a comparative good organic chelator to sensitize fluorescence of Tb(III) ion.

3.4. Analysis of the interaction of complex with BSA

BSA has been studied as a model protein due to its structural homology with human serum albumin [14]. There are three types of fluorophores in BSA, namely tryptophan residues (Trp), tyrosine residues (Tyr), and phenylalanine residues. Although both Trp and Tyr residues can be excited at 280 nm, energy transfer effect at 280 nm mostly comes from Trp residues [19]. At the excitation wavelength of 280 nm, BSA exhibits a strong fluorescence emission with a peak at around 340 nm [20].

3.4.1. Analysis of fluorescence quenching of BSA by the complex

Fluorescence quenching is the decrease of the quantum yield of fluorescence from a fluorophore induced by a variety of molecular interactions with quencher molecules. Under the conditions of fixed pH, temperature and ionic strength, fluorescence quenching may result from exciting-state reaction, molecular rearrangements, energy transfer, ground complex formation and collisional quenching processes [21]. Fluorescence quenching can be dynamic which results from collisional encounters between the fluorophore and quencher, or static, owing to the formation of a ground state complex between the fluorophore and quencher [22]. In general, static and dynamic quenching can be distinguished from their different binding constants dependent on temperature and viscosity, or preferably by lifetime measurements.

The fluorescence spectra of BSA with increasing concentrations of the complex at 298 K when excited at 280 nm are illustrated in Fig. 3.

As shown in Fig. 3, the natural fluorescence of BSA at around 340 nm is gradually quenched by the increasing concentration of the complex, while the complex $Tb_2(L)_3{\cdot}5H_2O$ has no intrinsic fluorescence in this range. Results above indicate that there are strong interactions and radiationless energy transfer between BSA and the complex $Tb_2(L)_3{\cdot}5H_2O$ [23].

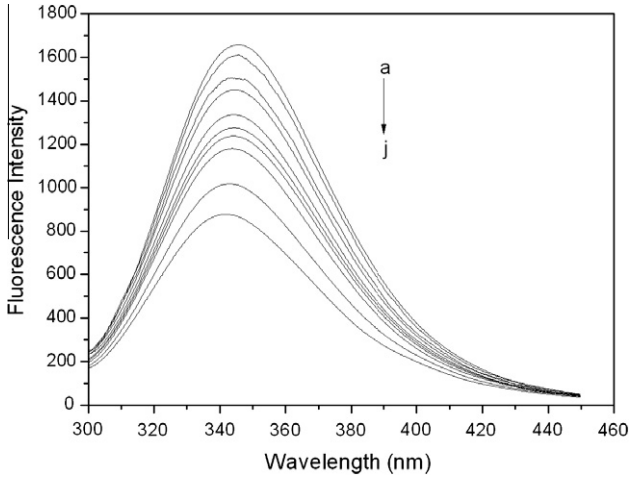

Fig. 3. Effect of $Tb_2(L)_3{\cdot}5H_2O$ on fluorescence spectrum of BSA. T = 298 K, pH = 7.4, λ_{ex} = 280 nm. c(BSA) = 1.0×10^{-5} mol/L, c($Tb_2(L)_3{\cdot}5H_2O$)/(10^{-5} mol/L), a–j: 0, 0.10, 0.15, 0.20, 0.30, 0.35, 0.40, 0.50, 0.75, 1.0.

In order to shed light on the fluorescence quenching mechanism, the fluorescence quenching data were analyzed by the Stern–Volmer equation (Eq. (1)) [20]. The graphs plotted for F_0/F against [Q] from Eq. (1) at different temperatures are shown in Fig. 4.

$$F_0/F = 1 + k_q\tau_0[Q] = 1 + Ksv[Q] \quad (1)$$

where k_q, Ksv, τ_0 and [Q] are the biomolecular quenching rate constant, the dynamic Stern–Volmer quenching constant, the average biomolecular lifetime in the absence of quencher at about 10^{-8} s [24], and the concentration of quencher, respectively. F_0 and F are the fluorescence intensities in the absence and presence of quencher, respectively. The biomolecular quenching rate constant k_q and the dynamic Stern–Volmer quenching constant Ksv at pH 7.40 can be obtained by the slope of the diagram at different temperatures, which are given in Table 4. In general, for the dynamic quenching, the quenching constant Ksv of the fluorescent complex increases with the temperature due to faster diffusion and larger amounts of collision quenching in the case of higher temperature. Furthermore, the maximum quenching rate constant k_q of various kinds of bimolecular is 2.0×10^{10} M^{-1} s^{-1} [25]. The quenching constant Ksv in Table 4 is inversely correlated with the temperature, and the quenching rate constant k_q is much larger than 2.0×10^{10} M^{-1} s^{-1}. This indicates that the quenching mechanism of fluorescence of BSA by the complex is not initiated by dynamic collision but the formation of a complex instead.

It is well known that UV–vis absorption measurement is a very simple method and applicable to explore the structural change and study the complex formation [26]. Therefore, to further confirm the quenching mechanism induced by the complex, we studied the difference of UV–vis absorption spectra of BSA in the absence and presence of the complex.

Fig. 5 shows the effect of increasing concentrations of the complex on the UV–vis absorption spectra of BSA. We can clearly see

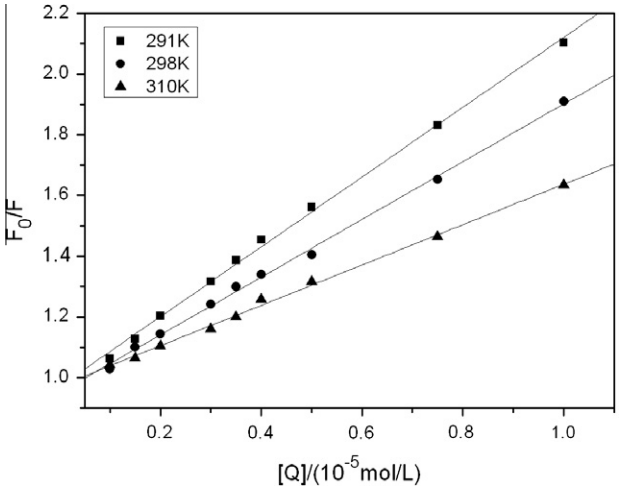

Fig. 4. The Stern–Volmer curves of BSA quenched by $Tb_2(L)_3{\cdot}5H_2O$.

Table 4
The quenching and dissociation constants of BSA with $Tb_2(L)_3{\cdot}5H_2O$ at different temperatures.

T (K)	Ksv (L mol^{-1})	k_q (L mol^{-1} s^{-1})	R^2
291	1.150×10^5	1.150×10^{13}	0.99741
298	0.951×10^5	0.951×10^{13}	0.99745
310	0.665×10^5	0.665×10^{13}	0.99712

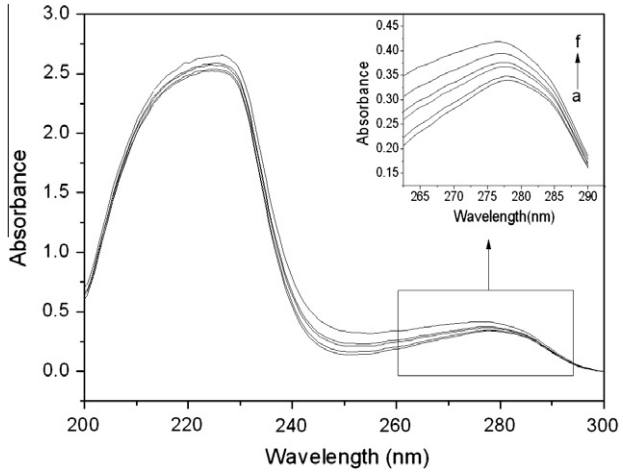

Fig. 5. Effect of $Tb_2(L)_3{\cdot}5H_2O$ on UV–vis absorption spectra of BSA. $T = 298$ K, pH = 7.4. c(BSA) = 1.0×10^{-5} mol/L, c($Tb_2(L)_3{\cdot}5H_2O$)/(10^{-5} mol/L), a–f: 0, 0.1, 0.15, 0.2, 0.25.

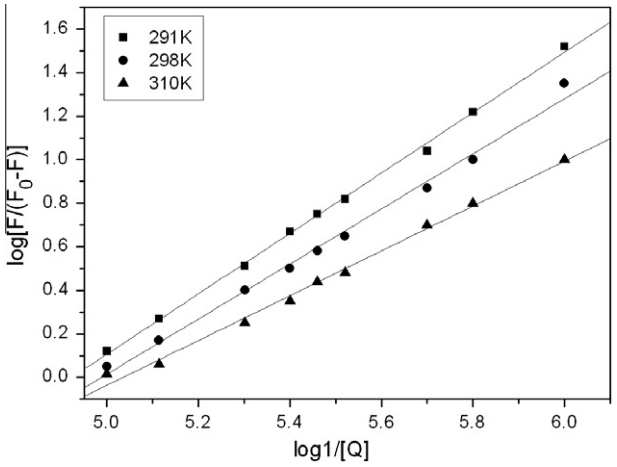

Fig. 6. Double-log plots of $Tb_2(L)_3{\cdot}5H_2O$ quenching effect on BSA fluorescence at different temperatures.

that the absorption of BSA is increased regularly around 280 nm with the addition of the complex, indicating that the complex $Tb_2(L)_3{\cdot}5H_2O$ has penetrated into the hydrophobic pocket of the Trp residues, which inevitably result in the gradual exposure of the Trp residues inside the hydrophobic cavities. It is responsible for the gradual increase of absorption [27]. Research consistently suggests the dynamic quenching only affects the excited state of fluorophore and does not change the absorption spectrum. However, the formation of non-fluorescence ground state complex induced the change of absorption spectrum of fluorophore [28]. It is clear that the mechanism of fluorescence quenching was a static quenching procedure.

3.4.2. Calculation of binding constants and binding sites

If the non-fluorescence ground state complex is formed between BSA and quencher, the apparent binding constant *Ka* ($L\,mol^{-1}$) and binding sites n can be expressed by the following equation [29]:

$$\log\frac{F}{F_0 - F} = \log\frac{1}{Ka} + n\log\frac{1}{[Q]} \tag{2}$$

where F_0 and F are the fluorescence intensities before and after the addition of the quencher and [*Q*] is the concentration of quencher. Based on the measured fluorescence data at different temperatures, the plots of $\log F/(F_0 - F)$ versus $\log 1/[Q]$ were obtained (Fig. 6). And then binding constants *Ka* and binding sites n of the complex with BSA obtained from the intercept and slope of the linear dependence of $\log F/(F_0 - F)$ on $\log 1/[Q]$ were listed in Table 5. The correlation coefficient was about 0.99, which proves that the interaction between the complex and BSA is in accordance with the site-binding model underlined in the above equation. The binding constants *Ka* were in the range of 10^5–10^6 $L\,mol^{-1}$, which means that the complex quenches the fluorescence emission of BSA with higher binding affinity and experiences a static quenching procedure. The corresponding binding sites *n* at the temperatures of 291 K, 298 K and 310 K were 1.38, 1.26 and 1.02, respectively, which roughly equal to 1, indicating the interaction of the complex with BSA has only a single binding site.

3.4.3. Thermodynamic parameters and nature of the binding forces

Research shows that the intermolecular forces between the quencher and biomolecular mainly include hydrophobic forces, electrostatic interactions, Van der Waals interactions and hydrogen bonds, etc. [30]. The thermodynamic parameters (enthalpy change

Table 5
The binding constants *Ka*, binding sites *n*, and the thermodynamic parameters at different temperatures for $Tb_2(L)_3{\cdot}5H_2O$–BSA system.

T (K)	*Ka* ($L\,mol^{-1}$)	*n*	R^2	ΔH ($kJ\,mol^{-1}$)	ΔS ($J\,mol^{-1}\,K^{-1}$)	ΔG ($kJ\,mol^{-1}$)
291	66.9×10^5	1.38	0.99807	−147.03	−374.36	−38.09
298	20.6×10^5	1.26	0.99214	−147.03	−374.36	−35.74
310	1.5×10^5	1.02	0.99338	−147.03	−374.36	−31.25

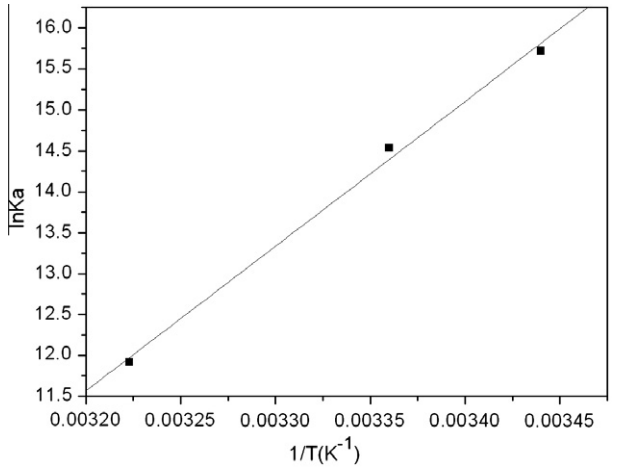

Fig. 7. Van't Hoff plot for the interaction of BSA and $Tb_2(L)_3{\cdot}5H_2O$.

ΔH and entropy change ΔS) were calculated from the Van't Hoff equation (Eq. (3)) at three different temperatures. If $\Delta H \approx 0$ and $\Delta S > 0$, the main force is hydrophobic interaction; if $\Delta H < 0$ and $\Delta S > 0$, the main force is electrostatic; if $\Delta H < 0$ and $\Delta S < 0$, Van der Waals and hydrogen bond interactions play major role in the reaction [31].

$$\ln Ka = -\Delta H/RT + \Delta S/R \tag{3}$$

where *Ka* is the effective binding constant at the corresponding temperature and *R* is the universal gas constant. If the enthalpy change ΔH does not vary significantly over the temperature range studied, ΔH can be regarded as a constant. The plot of $\ln Ka$ versus $1/T$ is shown in Fig. 7 The enthalpy change ΔH and entropy change ΔS were obtained from the slope and intercept of the fitting curve,

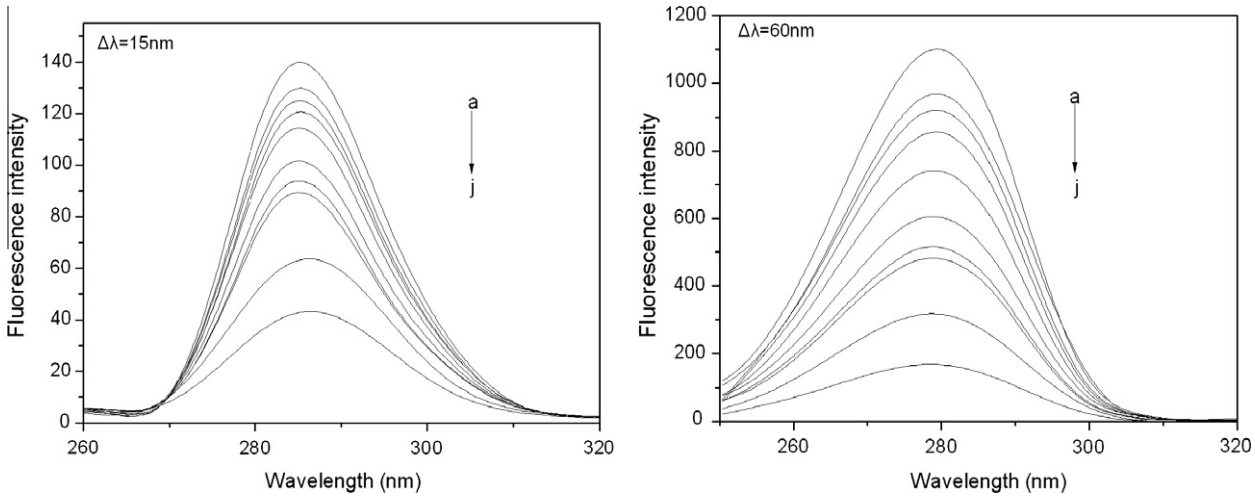

Fig. 8. Effect of $Tb_2(L)_3{\cdot}5H_2O$ on the synchronous fluorescence spectra of BSA. T = 298 K, pH = 7.4. c(BSA) = 1.0×10^{-5} mol/L, c($Tb_2(L)_3{\cdot}5H_2O$)/(10^{-5} mol/L), a–j: 0, 0.10, 0.15, 0.20, 0.30, 0.35, 0.40, 0.50, 0.75, 1.0.

respectively. The free energy change can be obtained from the following relationship:

$$\Delta G = \Delta H - T\Delta S \quad (4)$$

The values of thermodynamic parameters are presented in Table 5. The ΔH and ΔS values are in accordance with the reported literature [32]. The negative free energy change ΔG suggests that the binding process is spontaneous. The negative values of enthalpy ΔH and entropy ΔS suggest that the binding is mainly enthalpy driven and the entropy is unfavorable for it, hydrogen bonds and van der Waals interactions played major roles in reaction [31].

3.4.4. Synchronous fluorescence spectra

The synchronous fluorescence spectra can provide much valuable information about the microenvironment in the vicinity of the chromophore molecules [33]. According to Miller [34], distinction of the difference between excitation wavelength and emission wavelength ($\Delta\lambda = \lambda_{emi} - \lambda_{exc}$) reflects the spectra of a different nature of chromophores. When $\Delta\lambda$ values are stabilized at 15 or 60 nm, the synchronous fluorescence of BSA is characteristic of tyrosine or tryptophan residue [35]. The effect of $Tb_2(L)_3{\cdot}5H_2O$ on BSA synchronous fluorescence spectroscopy is shown in Fig. 8 It can be seen that the fluorescence intensities at $\Delta\lambda$ = 15 nm and $\Delta\lambda$ = 60 nm are both decreased more and more seriously with increasing concentration of $Tb_2(L)_3{\cdot}5H_2O$. Moreover, a notable red shift of maximum emission wavelength of tyrosine residue are observed upon addition of $Tb_2(L)_3{\cdot}5H_2O$, whereas the tryptophan residue emission maximum keep unchanged. This red shift (from 284 nm to 287 nm) indicates that the conformation of BSA is changed, resulting in the increase of polarity of the fluorophore environment. This increased polarity is probably due to the hydrogen bonding between the $Tb_2(L)_3{\cdot}5H_2O$ and BSA.

4. Conclusion

In summary, a novel aromatic β-diketone ligand, 4-isopropyl-2,6-bisbenzoylactyl pyridine and its complex $Tb_2(L)_3{\cdot}5H_2O$ were synthesised and characterized. The FT-IR spectra difference between ligand and complex indicated that the coordination of the metal ions to the ligand occurred at the oxygen atoms of the enol-form group. Furthermore, the study of the luminescence properties of the complex showed the Tb(III) could be sensitized efficiently by the ligand. In addition, the interaction between the complex $Tb_2(L)_3{\cdot}5H_2O$ and BSA has been investigated by fluorescence method and supplemented by UV–vis under simulative physiological pH conditions. The fluorescence quenching results showed that the intrinsic fluorescence of BSA was quenched through static quenching mechanism. The binding constants and the number of binding sites at different temperatures were also obtained, which revealed the interaction of the complex with BSA has only a single binding site. The values of thermodynamic parameters and the synchronous fluorescence spectra confirmed that the hydrophobic and hydrogen bond interactions played a significant role in the formation of complex $Tb_2(L)_3{\cdot}5H_2O$–BSA coordination compound. This study is expected to be useful to understand the mechanism of interactions of the rare earth complex binding to BSA and provide important information for theoretical research and application in drug pharmacokinetic and pharmacodynamic fields.

Acknowledgment

This work was financially supported by the National Natural Science Foundation of China (No. 21071152).

References

[1] V. Tsaryuk, V. Zolin, K. Zhuravlev, V. Kudryashova, J. Legendziewicz, R. Szostak, J. Alloys Compd. 451 (2008) 153.
[2] J. Kido, Y. Okamoto, Chem. Rev. 102 (2002) 2357.
[3] R.X. Ma, Z.M. Chen, Z.H. Gao, R.F. Wang, J.J. Zhang, Syn. Met. 159 (2009) 1272.
[4] E. Niyama, H.F. Brito, M. Cremona, Spectrochim. Acta Part A 61 (2005) 2643.
[5] C.M.G. dos Santos, A.J. Harte, S.J. Quinn, T. Gunnlaugsson, Coordin. Chem. Rev. 252 (2008) 2512.
[6] B.L. An, M.L. Gong, M.X. Li, J.M. Zhang, Z.X. Cheng, J. Fluorescence 15 (2005) 613.
[7] Y.G. Lv, J.C. Zhang, W.L. Cao, J.C. Juan, F.J. Zhang, Z. Xu, J. Photochem. Photobiol. A 188 (2007) 155.
[8] S.B. Meshkova, J. Fluorescence 10 (2000) 333.
[9] Y.M. Luo, J. Li, L.X. Xiao, R.R. Tang, X.C. Tang, Spectrochim. Acta Part A 72 (2009) 703.
[10] R.R. Tang, W. Zhang, Y.M. Luo, J. Li, J. Rare Earth. 27 (2009) 362.
[11] G. Zolese, G. Falcioni, E. Bertoli, R. Wozniak, Z. Wypych, E. Gratton, A. Ambrosini, Proteins 40 (2000) 39.
[12] C.P. Montgomery, E.J. New, D. Parker, R.D. Peacock, Chem. Comm. 36 (2008) 4261.
[13] P. Caravan, N.J. Cloutier, M.T. Greenfield, S.A. McDermid, S.U. Dunham, J.W.M. Bulte, J.C. Amedio, R.J. Looby, R.M. Supkowski, W. DeW. Horrocks, T.J. McMurry, R.B. Lauffer, J. Am. Chem. Soc. 124 (2002) 3152.
[14] K.S. Ghosh, S. Sen, B.K. Sahoo, S. Dasgupta, Biopolymers 91 (2009) 737.
[15] R. Shelkov, A. Melman, Eur. J. Org. Chem. 2005 (2005) 1397.
[16] H.X. Wu, C.Y. Xi, Q.Z. He, Z.M. Wang, Chin. J. Spectrosc. Lab. 22 (2005) 260.
[17] L.X. Xiao, Y.M. Luo, Z. Chen, J. Li, R.R. Tang, Spectrochim. Acta Part A 71 (2008) 321.

[18] R.R. Tang, C.H. Tang, C.Q. Tang, J. Organomet. Chem. 696 (2011) 2040.
[19] A. Sułkowska, M. Maciazek-Jurczyk, B. Bojko, J. Mol. Struct. 881 (2008) 97.
[20] J.R. Lakowicz, Principles of Fluorescence Spectroscopy, second ed., Plenum Press, New York, 1999.
[21] B. Valeur, Molecular Fluorescence. Principles and Applications, Wiley Press, NY, 2001.
[22] X.J. Guo, X.W. Han, J. Tong, C. Guo, W.F. Yang, J.F. Zhu, B. Fu, J. Mol. Struct. 966 (2010) 129.
[23] X.L. Lu, J.J. Fan, Y. Liu, A.X. Hou, J. Mol. Struct. 934 (2009) 1.
[24] J.R. Lakowicz, G. Weber, Biochemistry 12 (1973) 4161.
[25] W.R. Ware, J. Phys. Chem. 66 (1962) 455.
[26] S. Ashoka, J. Seetharamappa, P.B. Kandagal, S.M.T. Shaikh, J. Lumin. 121 (2006) 179.
[27] A. Papadopoulou, R.J. Green, R.J. Frazier, J. Agric. Food Chem. 53 (2005) 158.
[28] H.Y. Liu, Z.H. Xu, X.H. Liu, P.X. XI, Z.Z. Zeng, Chem. Pharm. Bull. 57 (2009) 1237.
[29] J. Kang, Y. Liu, M.X. Xie, S. Li, M. Jiang, Y.D. Wang, BBA – Gene Subj. 1674 (2004) 205.
[30] Y.N. Ni, G.L. Liu, S. Kokot, Talanta 76 (2008) 513.
[31] P.D. Ross, S. Subramanian, Biochemistry 20 (1981) 3096.
[32] U. Katrahalli, S. Jaldappagari, S.S. Kalanur, J. Lumin. 130 (2010) 211.
[33] B. Klajnert, M. Bryszewska, Bioelectrochemistry 55 (2002) 33.
[34] J.N. Miller, Proc. Anal. Div. Chem. Soc. 16 (1979) 203.
[35] J.H. Tang, F. Luan, X.G. Chen, Bioorg. Med. Chem. 14 (2006) 3210.